Proceedings of the ASME 2014 International Mechanical Engineering Congress & Exposition
IMECE2014
November 14-20, 2014, Montreal, Quebec, Canada

IMECE2014-38396

MODELING OF NEAR-FIELD CONCENTRATED SOLAR THERMOPHOTOVOLTAIC MICROSYSTEM

Mahmoud Elzouka
University of Nebraska - Lincoln
Mechanical and Materials Engineering Department
Lincoln, Nebraska, 68588-0526
USA
+1 402 419 9260, melzouka2@unl.edu

Mukesh Kulsreshath
University of Nebraska - Lincoln
Mechanical and Materials Engineering Department
Lincoln, Nebraska, 68588-0526
USA
mukesh.kulsreshath@unl.edu

Sidy Ndao
University of Nebraska - Lincoln
Mechanical and Materials Engineering Department
Lincoln, Nebraska, 68588-0526
USA
sndao2@unl.edu

ABSTRACT

Modeling of a near-field concentrated solar thermophotovoltaic (STPV) microsystem is carried out to investigate the use of STPV-based solid-state energy conversion as a high power density MEMS power generator. Near-field radiation can be realized between two closely separated surfaces (i.e. order of radiation wavelength), resulting in the enhancement of the heat radiation flux orders of magnitudes higher than the blackbody limit, consequently increasing cell output power density. The Near-field STPV model consists of an absorber/emitter model used to estimate the net power absorbed from solar irradiance, a near-field radiation transfer model to evaluate the power tunneled from the emitter to the PV cell at different separation distances, and a PV cell model to determine the photocurrent generated due to thermal radiation absorbed. Results reveal that decreasing separation distance between the emitter and the PV cell increases the absorber/emitter thermal efficiency, increases conversion efficiency, and the power density (×100 far-field). The results also predict increase in cooling power requirement as the separation distance is decreased, which may be a limiting design parameter for near-field STPV microsystems. Based on the model, an overall conversion efficiency of 17% at a separation distance of 10 nm and emitter temperature of 2000 K with solar concentration 6000 sun can be reached; this corresponds to an output power density of 9×10^5 W/m^2.

INTRODUCTION

The world market for products incorporating micro and nanosystems is expected to exceed $1 trillion dollars by 2020. This trend, along with global efforts to reduce our carbon footprint in favor of using renewable energy sources such as the sun, points to the need for research in small-scale, solid-state, and clean energy-based portable power generation for integrated micro/nanosystem devices such as consumer portable electronics, remote sensing devices, unmanned aerial vehicles, autonomous robots, and BioMEMS devices. One of the most promising portable power generation alternative to batteries and microengines is near-field radiation transfer enabled concentrated solar thermophotovoltaic (STPV) microsystem. Unlike conventional solar photovoltaics, a concentrated STPV system converts solar radiation to electricity using heat as an intermediary through a thermally coupled absorber/emitter (Fig. 1-a) and has one of the highest solar-to-electricity conversion efficiency limits (~85.4%) while presenting opportunities for thermal storage though practical efficiencies of STPV converters are 20 – 30% [1] with much lower values at the microscale.

While conventional PV systems only utilize a portion of the solar spectrum efficiently, STPVs can overcome the Shockley-Queisser single-junction PV limit [2], [3]. This can be illustrated by investigating the PV cell quantum efficiency (Fig. 1-b) which is maximum just above band-gap photon energy; hence it is beneficial to illuminate the PV cell with radiation within that range. Wide solar spectrum can be converted to a narrower one by introducing an intermediate surface between the solar radiation and PV cell to modify the spectrum (Fig. 1), hence the concept of thermophotovoltaics. The intermediate surface absorbs the solar radiation to be then converted to thermal energy and reemitted towards the PV cell via thermal radiation which inherently has a narrower spectrum than the solar radiation. Choosing a PV cell with band gap energy matching the thermal radiation spectrum will lead to enhancement in the overall conversion efficiency. STPV is also considered more flexible than conventional SPV as it can be operated with external heat source (i.e. combustion) in the absence of solar irradiance. STPV has been investigated theoretically and experimentally; a comprehensive review of the literature can be found in [4].

Most recent efforts in improving the performance of STPVs aim to develop selective absorbers and emitters either by choosing proper material with a favorable inherent selective emission [5] or through surface nanoengineering (e.g., Photonic crystals) [6]–[8]. In the present research, we investigate the effect of near-field thermal radiation to boost performance of STPV; it is important to note that such study has not been performed yet in the open literature. Near-field thermal radiation transfer becomes important when the spacing (optical cavity spacing) between the emitter and the PV cells is reduced to below the characteristic wavelength of thermal radiation. Conventional TPV systems generally have optical cavity spacing in the order of a few millimeters thus limited by Plank's blackbody radiation. Thermally excited electromagnetic waves are of two types, namely, propagating waves and evanescent waves. Plank's law of blackbody radiation only accounts for propagating electromagnetic waves. On the other hand, evanescent waves are non-propagating waves that decay away from a radiating surface. However when two objects are brought close enough within a distance proportional to the nominal wavelength of thermal radiation, near-field effects due to the tunneling of evanescent waves become important, resulting in the enhancement of radiative heat transfer above Plank's blackbody limit.

Near-field radiative heat transfer has been extensively studied theoretically and recently a few experimental methods for measuring the near-field transfer have been proposed. Kittel et al. [9] performed measurements of the near-field heat transfer between the tip of a thermal profiler and planar material surfaces, their results agree with theoretical calculations above 10 nm. Hu et al. [10] reported measurement of radiative heat transfer between parallel glass surfaces separated by nanoparticels. Their measured heat transfer exceeded what's predicted by Planck's blackbody law. Shen et al. [11] measured the heat flux between a microsphere and a flat surface separated by 30 nm. The corresponding heat transfer coefficients at such distance are 3 orders of magnitude larger than that of the blackbody radiation limit.

Near-field TPV has been also investigated in literature theoretically and experimentally [12]. Basu et al. [13] provided a thorough review of the applications of near-field TPV devices to energy conversion, including their advantages over current technologies. A recent near-field TPV numerical model is presented in [14] and [15]. A very recent experimental work has demonstrated the feasibility of near-field TPV [12] with reported performance improvements of up to a 10x increase in power density, 30% to 35% fractional increase in conversion efficiency, or alternatively reduced radiator temperature requirements to as low as 550 ^{o}C based on a 0.55 eV InGaAs diode.

In the present study, modeling of a near-field concentrated solar thermophotovoltaic (STPV) is presented for the first time in the literature. The model consists of three interdependent parts. The first is modeling of absorber/emitter to estimate the net energy absorbed from the incident solar irradiance. This depends on losses to the environment and the amount of energy tunneled to the PV cell by near-field radiation. The second is the near-field thermal radiation power transfer from emitter to PV cell, which incorporates fluctuation dissipation theorem to find out the effect of near-field radiation. The third is the modeling of PV cell to find out the photocurrent generated corresponding to absorbed thermal radiation from the emitter. The photocurrent calculation considers local electron/hole (EH) generation due to thermal radiation absorption through the PV cell and minority carrier recombination.

NOMENCLATURE

$\overline{\overline{\boldsymbol{G}}}^{E}$	Electric dyadic Green's function
$\overline{\overline{\boldsymbol{G}}}^{H}$	Magnetic dyadic Green's function
D_h	Carrier diffusion coefficient for holes
D_e	Carrier diffusion coefficient for electrons
E_b	Blackbody emissive power
J_0	Dark current
J_{ph}	Photoelectric current
$L_{dp,n}$	Depletion region width in n-doped region
$L_{dp,p}$	Depletion region width in p-doped region
N_a	Acceptor concentration
N_d	Donor concentration
$P_{electric}$	Output electric power from PV cell
P_m	Maximum PV cell output electric power
$Q_{PV \rightarrow emitter}$	Net radiation power emitted from PV cell to emitter surface

$Q_{cooling}$	Heat rejecting from the PV cell
$Q_{emitter}$	Total net power absorbed by emitter
$Q_{emitter \rightarrow PV}$	Net radiation power emitted from emitter surface to PV cell
$Q_{loss,Env}$	Total heat lost by absorber to the environment
$Q_{solar,abs}$	Total absorbed solar radiation
$Q_{solar,inc}$	Total incident solar radiation
$Q_{solar,ref}$	Total reflected solar radiation
S_h	Minority holes surface recombination rate
S_e	Minority electrons surface recombination rate
T_c	PV cell temperature
T_e	Emitter temperature
V_0	Equilibrium built-in voltage of p-n junction
V_f	Forward bias voltage
d_c	Separation distance between emitter and PV cell
k_b	Boltzmann constant
$k_{z,1}$	Component of wave vector normal to the surface (in z direction)
$k''_{z,1}$	Imaginary component of Component of wave vector normal to the surface
k_v	Wave vector in vacuum
k_ρ	Component of wave vector parallel to the surface
n_0	Equilibrium electron concentration
n_{suns}	Solar concentration
p_0	Equilibrium hole concentration
$q_{solar,inc}$	Spectral incident solar radiation
z_c	Coordinate of point where radiation is calculated
$z_{dp,n}$	Coordinate of depletion region edge in n-doped region
$z_{dp,p}$	Coordinate of depletion region edge in p-doped region
$\hbar$	Circular Planck's constant
Δn	Excess minority electrons concentration
Δp	Excess minority holes concentration
$G(z,\omega)$	Local electron/hole generation rate for a given photon frequency
V	Body volume
e	Electron charge (elementary charge)
x	Fraction of Ga in the alloy $In_{1-x}Ga_xSb$
$\boldsymbol{E}$	Electric field vector
$\boldsymbol{H}$	Magnetic field vector
$\boldsymbol{J}$	Local thermally induced current density vector
$\boldsymbol{S}$	Poynting vector
$\boldsymbol{r}$	Position vector

Greek

ε''_r	Imaginary component of relative permittivity
ε_v	Vacuum permittivity
η_{STPV}	Conversion efficiency of solar thermophotovoltaic cell
η_{TPV}	Conversion efficiency of thermophotovoltaic cell
$\eta_{absorber/emitter}$	Absorber/emitter efficiency
η_q	Quantum efficiency
λ_T	Wavelength of peak thermal radiation
$\mu_{e,h}$	Mobility of minority electrons/holes
μ_v	Vacuum permeability
τ_h	Minority holes lifetime
τ_e	Minority electrons lifetime
ω_g	Band-gap frequency
$\hbar$	Circular Planck's constants
Θ	mean energy of Planck's oscillator
δ	Dirac-delta function
ε	Dielectric function
ρ	Spectral reflectivity
ω	Radiation angular frequency (rad/s)
ϵ	Spectral emissivity

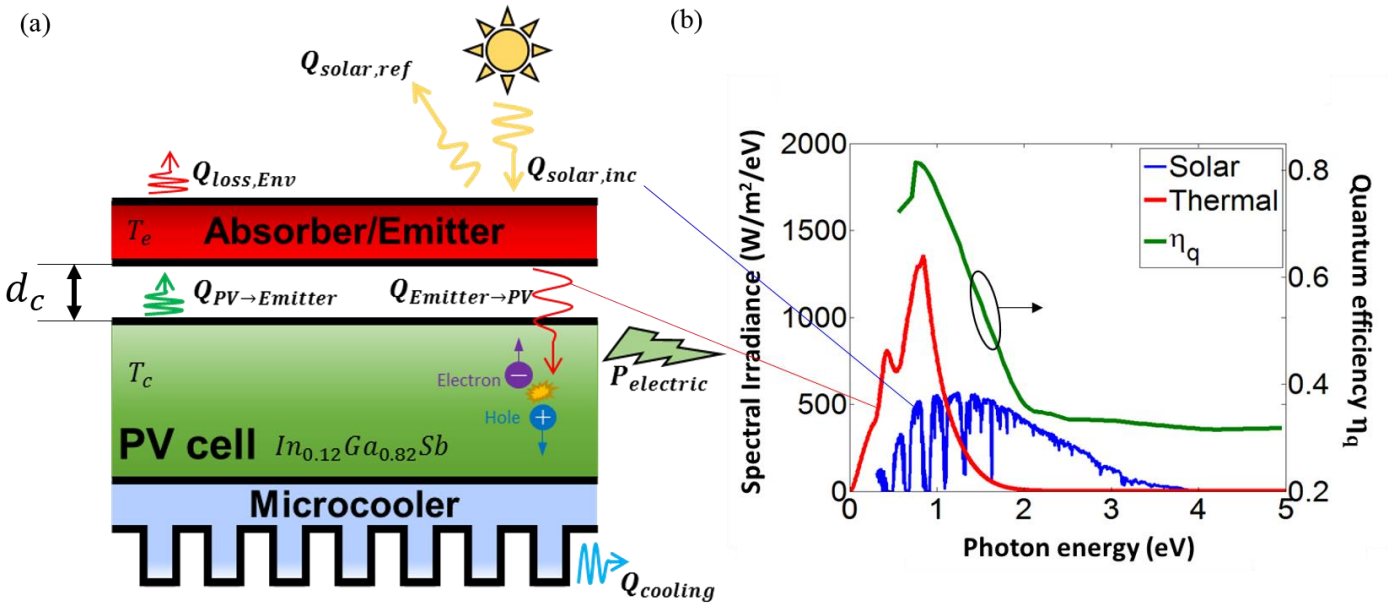

Fig. 1: Solar Thermophotovoltaic system layout. a) Layout of near-field solar thermophotovoltaic cell incorporating energy components: $Q_{solar,inc}$ solar incident power, $Q_{solar,ref}$ solar reflected energy, $Q_{loss,env}$ power loss to environment from absorber surface, $Q_{emitter\rightarrow PV}$ power from emitter surface to PV cell, $Q_{PV\rightarrow emitter}$ power from PV cell to emitter, $P_{electric}$ electrical power output from the cell and $Q_{cooling}$ heat rejecting from the PV cell due to losses mechanisms. b) solar spectrum (AM 1.5D) compared to near-field radiation spectrum with the same total integrated power, both compared to the cell quantum efficiency

THEORY

Near-Field Thermal Radiation

Thermal radiation is customary treated as a surface phenomenon which is analyzed using the concept of surface emissivity [16]. This approach is quite acceptable when the problem characteristic dimension is much larger than radiation dominating wavelength. But when this condition is violated, we should consider the origin of radiation as a bulk phenomenon. Thermal radiation is inherent in bulk of all kind of material, it is resulted from the field generated due to chaotic motion of charges within materials. This can be considered as small dipoles with random amplitudes and directions [13]. The spacing effect on the net heat transfer arises from two effects that are interrelated [13]. The first is wave interference due to multiple reflections inside the separation distance d_c that is important when it is close to but greater than λ_T. The second is due to photon tunneling that contributes significantly to near-field energy transfer when $d_c < \lambda_T$. This photon tunneling is a result of total internal reflection [17]. To investigate radiation as a bulk phenomenon, radiation should be dealt with as electromagnetic wave via fluctuation-dissipation theorem. According to the fluctuation–dissipation theorem, thermal emission is originated from the fluctuating currents induced by the random thermal motion of charges, known as thermally induced dipoles [18]. This current induces electromagnetic wave which can be estimated via Maxwell equations. The fluctuation electrodynamics combines the fluctuation–dissipation theorem with Maxwell's equations to fully describe the emission, propagation, and absorption of thermal radiation in both the near and far field [18]. The random thermal fluctuations produce a spatial- and time-dependent electric current density $\boldsymbol{J}(x,t)$ inside the medium whose time average is zero (otherwise any hot body will experience net electric current).

The most common technique adopted in near-field thermal radiation calculations is to express the fields in terms of dyadic Green's functions (DGFs). Using the method of potentials [19], [20], the electric and magnetic fields can be expressed as:

$$\boldsymbol{E}(\boldsymbol{r},\omega) = i\omega\mu_v \int_V dV' \overline{\overline{\boldsymbol{G}}}^E(\boldsymbol{r},\boldsymbol{r}',\omega).\boldsymbol{J}^r(\boldsymbol{r}',\omega) \tag{1}$$

$$\boldsymbol{H}(\boldsymbol{r},\omega) = \int_V dV' \overline{\overline{\boldsymbol{G}}}^H(\boldsymbol{r},\boldsymbol{r}',\omega).\boldsymbol{J}^r(\boldsymbol{r}',\omega) \tag{2}$$

And the ensemble average of the fluctuating current densities is given by [18]

$$\langle \boldsymbol{J}_\alpha^r(\boldsymbol{r}',\omega)\boldsymbol{J}_\beta^{r\,*}(\boldsymbol{r}'',\omega')\rangle = \frac{\omega\varepsilon_v\varepsilon_r''(\omega)}{\pi}\Theta(\omega,T)\delta(r'-r'')\delta(\omega-\omega')\delta_{\alpha\beta} \tag{3}$$

where $\Theta(\omega,T)$ is the mean energy of Planck's oscillator,

$$\Theta(\omega, T) = \frac{\hbar\omega}{\exp(\hbar\omega/k_b T) - 1} \quad (4)$$

subscripts α and β are to indicate two different direction of thermally induced current, $\delta(r' - r")$ is to translate the assumption that fluctuations at two different points are correlated in the limit $r" \to r'$, $\delta(\omega - \omega')$ is to indicate that spectral components of fluctuation currents are uncorrelated and $\delta_{\alpha\beta}$ accounts for the assumption of isotropic media. To find out the energy flux accompanies electromagnetic wave propagation, Poynting vector is calculated [21]

$$\langle \boldsymbol{S}(\boldsymbol{r}, \omega) \rangle = 4 * \frac{1}{2} * Re\{\langle \boldsymbol{E}(\boldsymbol{r}, \omega) \times \boldsymbol{H}^*(\boldsymbol{r}, \omega) \rangle\} \quad (5)$$

This expression of the Poynting vector is four times larger than its customary definition, since only the positive frequencies are considered in the Fourier decomposition of the time-dependent fields into frequency-dependent quantities [17]. Substitution of equations (1), (2) and (3) in equation (5), analytic integration along the source volume, and considering the z component of Poynting vector (due to azimuthal symmetry), we get equation (7) [22], where $q_{1\to2}(z_c, \omega)$ is the monochromatic radiative heat flux calculated from an arbitrary body 1 (emitter) to a body 2 (receiver) at location $z = z_c$ in body 2 along the *z*-direction, due to a semi-infinite radiation source (body 1) and g are components of dyadic green function.

In our STPV model, Tungsten is used as the emitter and its dielectric constant is taken from [23], while for PV cell semiconductor, $In_{1-x}Ga_xSb$ is used, which dielectric constant was calculated using the dielectric constant for GaSb and InSb combined with Vegard's law:

$$\varepsilon_{alloy}(x) = x\varepsilon_{GaSb} + (1 - x)\varepsilon_{InSb} - x(1 - x)C_B \quad (6)$$

where C_B is the so-called bowing constant that accounts for deviations from the linear interpolation due to lattice disorders [24]. Bowing constant is this case is omitted. For InSb and GaSb, dielectric constants are from [25].

Photovoltaic cell

The purpose of modeling PV cell is to find out the output photocurrent corresponding to a local thermal radiation absorption. It is found from theoretical and semi-empirical modeling that for an STPV illuminated with black body with temperature 1500 – 1800 ^{0}C, the optimum range of band-gap energy of PV cell is 0.4 – 0.6 eV [1]. One of the options is to use a ternary alloy, $In_{1-x}Ga_xSb$, which has a band gap that ranges from 0.18 eV (for pure InSb) to 0.72 eV (for pure GaSb) depending on the relative amount of indium and gallium in the compound. For this study, $In_{0.18}Ga_{0.82}Sb$ composition is used which has band-gap energy of 0.56 eV [26].

Current generated as a response of cell illumination can be estimated once minority carrier distribution is known, this is calculated by solving excess minority carrier steady state diffusion equation (i.e. electrons in p-doped sides and holes in the n-doped side) [27],

$$\mathrm{D_e}\frac{\partial^2 \Delta \mathrm{n(z,\omega)}}{\partial \mathrm{z}^2} + \mathrm{G(z,\omega)} - \frac{\Delta \mathrm{n(z,\omega)}}{\tau_e} = 0 \quad (8)$$

$$D_h \frac{\partial^2 \Delta p(z,\omega)}{\partial z^2} + G(z,\omega) - \frac{\Delta p(z,\omega)}{\tau_h} = 0 \quad (9)$$

which is valid for low injection conditions and no external voltage. The term $D\frac{\partial^2 \Delta}{\partial z^2}$ is the carrier conservation term, $G(z, \omega)$ the local generation rate of carrier and $\frac{\Delta}{\tau}$ is the recombination rate of excess minority carriers (i.e. sink term). Estimation of minority carrier diffusion coefficients D_e and D_h by relating them to carrier mobility via Einstein's relation:

$$D_{e,h} = \frac{\mu_{e,h} k_b T_c}{e} \quad (10)$$

Diffusion coefficient is estimated for minority holes $D_h = 18.3\ cm^2/s$ and for minority electrons $D_e = 35.18\ cm^2/s$. For InGaSb carrier mobility, it was calculated from Vegard's law,

$$q_{1\to2}(z_c, \omega) = \frac{k_v^2 \Theta(\omega, T)}{2\pi^2} Re\left\{ i\varepsilon''_{r,1}(\omega) \int_0^\infty \frac{k_\rho}{k''_{z,1}} \begin{bmatrix} g^E_{1\to2,\rho\rho}(k_\rho, z_c, \omega) g^{H*}_{1\to2,\theta\rho}(k_\rho, z_c, \omega) \\ +g^E_{1\to2,\rho z}(k_\rho, z_c, \omega) g^{H*}_{1\to2,\theta z}(k_\rho, z_c, \omega) \\ -g^E_{1\to2,\theta\theta}(k_\rho, z_c, \omega) g^{H*}_{1\to2,\rho\theta}(k_\rho, z_c, \omega) \end{bmatrix} dk_\rho \right\} \quad (7)$$

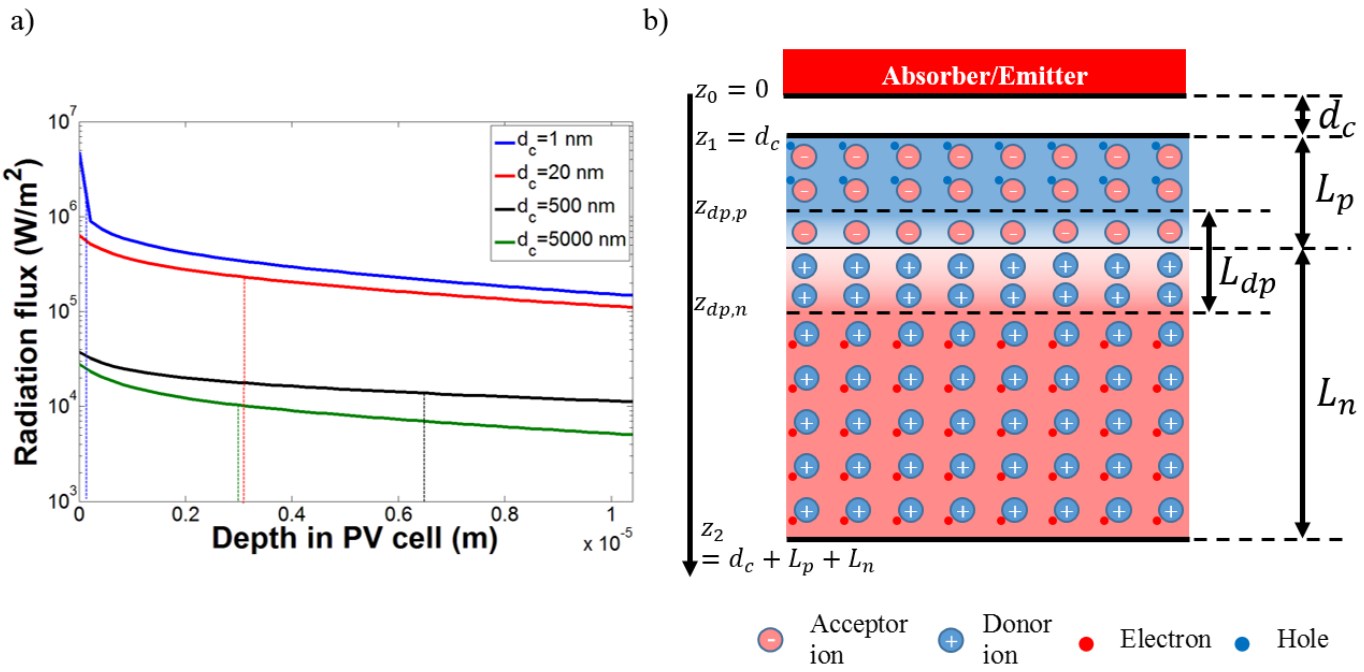

Fig. 2: TPV cell schematic – a) radiation flux through the PV cell depth, dotted vertical lines represent radiation penetration depth. b) PV cell composed of p-doped region (the upper half) with thickness $L_p = 0.4\ \mu m$ and dopant concentration $10^{19}\ cm^{-1}$ and n-doped region with thickness $L_n = 10\ \mu m$ and dopant concentration $10^{17}\ cm^{-1}$. The emitter is the solid body above the PV cell at distance d_c from the cell.

InSb and GaSb mobility was calculated from [27]. Generation rate of electron hole pairs as a result of thermal radiation absorption is given by [14]

$$G(z,\omega) = -\frac{1}{\hbar\omega}\frac{\partial \mathrm{q}(z,\omega)}{\partial z} \tag{11}$$

where $\frac{\partial \mathrm{q}(z,\omega)}{\partial z}$ represents radiation power absorbed per unit volume surrounding an element sliced at depth z. Minority carrier lifetime τ has three components corresponding to recombination mechanisms; SRH non-radiative recombination, non-radiative Auger recombination and radiative recombination. For $In_{0.18}Ga_{0.82}Sb$ at 300 K, the total minority carrier lifetimes of electrons and holes are 5.5 ns and 30.3 ns respectively [22].

Minority carrier diffusion equation is solved outside the depletion region for p-doped and n-doped separately with the following boundary conditions [22]:

$$\Delta n\left(z_{dp,p},\omega\right) = 0,\ D_e \frac{\partial \Delta n(z,\omega)}{\partial z}\Big|_{z=z_1} = S_e \Delta n \tag{12}$$

$$\Delta p\left(z_{dp,n},\omega\right) = 0,\ D_h \frac{\partial \Delta p(z,\omega)}{\partial z}\Big|_{z=z_2} = -S_h \Delta p \tag{13}$$

for p-doped and n-doped region, respectively, where S_e and S_h are surface recombination velocities for the minority electron or hole respectively, they depend on the material and surface treatment and it is difficult to determine precise values for them. For this calculation, $S_e = 2 * 10^4\ m/s$ and $S_h = 0$ [22].

Depletion region thickness for p-doped and n-doped region are respectively [28]

$$L_{dp,p} = \left(\frac{2\varepsilon_s V_0}{e}\left(\frac{N_d}{N_a(N_a+N_d)}\right)\right)^{0.5} \tag{14}$$

$$L_{dp,p} = \left(\frac{2\varepsilon_s V_0}{e}\left(\frac{N_a}{N_d(N_a+N_d)}\right)\right)^{0.5} \tag{15}$$

Where V_0 is the p-n junction equilibrium built-in voltage

$$V_0 = \frac{k_b T_c}{e}\ln\left(\frac{N_a N_d}{N_i^2}\right) \tag{16}$$

, T_c is PV cell temperature (assumed constant at 300 K) and ε_s is the static relative permittivity calculated by [27]

$$\varepsilon_s = (16.8 - 1.1x)\varepsilon_0 \tag{17}$$

Solving excess minority carriers diffusion equation lead to calculation of photocurrent for the PV cell, which has three components: current from minority electrons in p-doped region,

current from minority holes in n-doped region and current from electron hole pairs generated within the depletion region [22].

$$J_{ph,e}(\omega) = -eD_e \frac{\partial \Delta n}{\partial z}\Big|_{z_{dp,p}} \tag{18}$$

$$J_{ph,h}(\omega) = eD_h \frac{\partial \Delta p}{\partial z}\Big|_{z_{dp,n}} \tag{19}$$

$$J_{ph,depletion}(\omega) = \int_{z_{dp,p}}^{z_{dp,n}} eG(z,\omega)dz \tag{20}$$

Total photocurrent generated can be determined by

$$J_{ph} = \int_{\omega_g}^{\infty} [J_{ph,e}(\omega) + J_{ph,h}(\omega) + J_{ph,depletion}(\omega)]d\omega \tag{21}$$

where ω_g is the frequency corresponding to cell band-gap energy. The actual output current is the difference between the photogenerated current and the dark current, which is the current generated when the cell is in dark condition (no electron/hole generation) due to the applied forward voltage. This dark current can be calculated by solving the minority carrier diffusion equation in dark conditions (no electron hole generation) [29]. Boundary conditions are the same as illuminated conditions, except the concentration of minority carriers on edges of depletion region are

$$\Delta p\left(z_{dp,n}\right) = p_0 \exp(eV_f/k_b T_{cell}) \tag{22}$$

$$\Delta \mathrm{n}\left(z_{dp,p}\right) = \mathrm{n}_0 \exp(eV_f/k_b T_{cell}) \tag{23}$$

where p_0 and n_0 are the equilibrium hole and electron concentrations respectively. The calculated dark current is a function of voltage only and independent from radiation frequency (as it is in condition of zero radiation) [29]. Actual output current w.r.t forward bias voltage is

$$J(V_f) = J_{ph} - J_0(V_f) \tag{24}$$

Cell performance is assessed via photocurrent generated, maximum power density (the maximum power generated with respect to V_f, i.e. $P_m = max(V_f * J(V_f))$) and cell conversion efficiency

$$\eta_{TPV} = P_m / q_{total,absorbed} \tag{25}$$

Absorber/Emitter

This is the interface between solar irradiance and the receiver PV cell; it absorbs the concentrated solar energy from one side, and emits to PV cell from the other side with tailored spectrum. The purpose of this absorber/emitter is to tailor the thermal radiation spectrum to match the PV cell band-gap to maximize the electron/hole generation for a given input radiation power.

Assuming that enclosure in a perfect vacuum for the sake of insulation and protection of emitter form oxidation, we can consider only radiative heat transfer in solving energy equation of the absorber/emitter. The receiver (the face facing the sun) absorbs portion of incident solar radiation, this portion is

$$Q_{solar,abs} = n_{suns} * \int_0^{\infty} \left(1 - \rho(\lambda)\right) * q_{solar,inc}(\lambda)d\lambda \tag{26}$$

where spectral emissivity is related to spectral reflectivity by $1 = \epsilon(\lambda) + \rho(\lambda)$ for opaque bodies. Receiver also loses heat to the surrounding at ambient temperature, this can be calculated as

$$Q_{loss,Env} = \int_0^{\infty} \epsilon(\lambda)(E_b(T_{emitter},\lambda) - E_b(T_{env},\lambda))d\lambda \tag{27}$$

where (absorber/emitter temperature is considered uniform). Net absorbed energy by absorber is then

$$Q_{absorber} = Q_{solar,abs} - Q_{loss,Env} \tag{28}$$

First law of thermodynamics dictates that the net radiated energy by the emitter equals the net radiation absorbed by the absorber (i.e. $Q_{absorber} = Q_{emitter}$). The net emitted energy to PV cell is the difference between net energy radiated by the emitter towards the PV cell $Q_{Emitter \to PV}$ and net energy radiated from PV cell towards the absorber $Q_{PV \to Emitter}$, which are calculated from near-field radiation transfer (equation (7)). Performance of absorber/emitter is evaluated by its efficiency; which is defined as the ratio between net thermal radiation energy transferred from the emitter to the PV cell to the total incident solar radiation

$$\eta_{absorber/emitter} = \frac{Q_{emitter}}{Q_{solar,inc}} = \frac{Q_{solar,abs} - Q_{loss,Env}}{Q_{solar,inc}} \tag{29}$$

Tungsten is used for Absorber/Emitter bulk, but its surface facing the sun is covered by 2D tantalum Photonic crystal to maximize solar energy absorption. Emissivity of the Photonic crystal is adopted from [7].

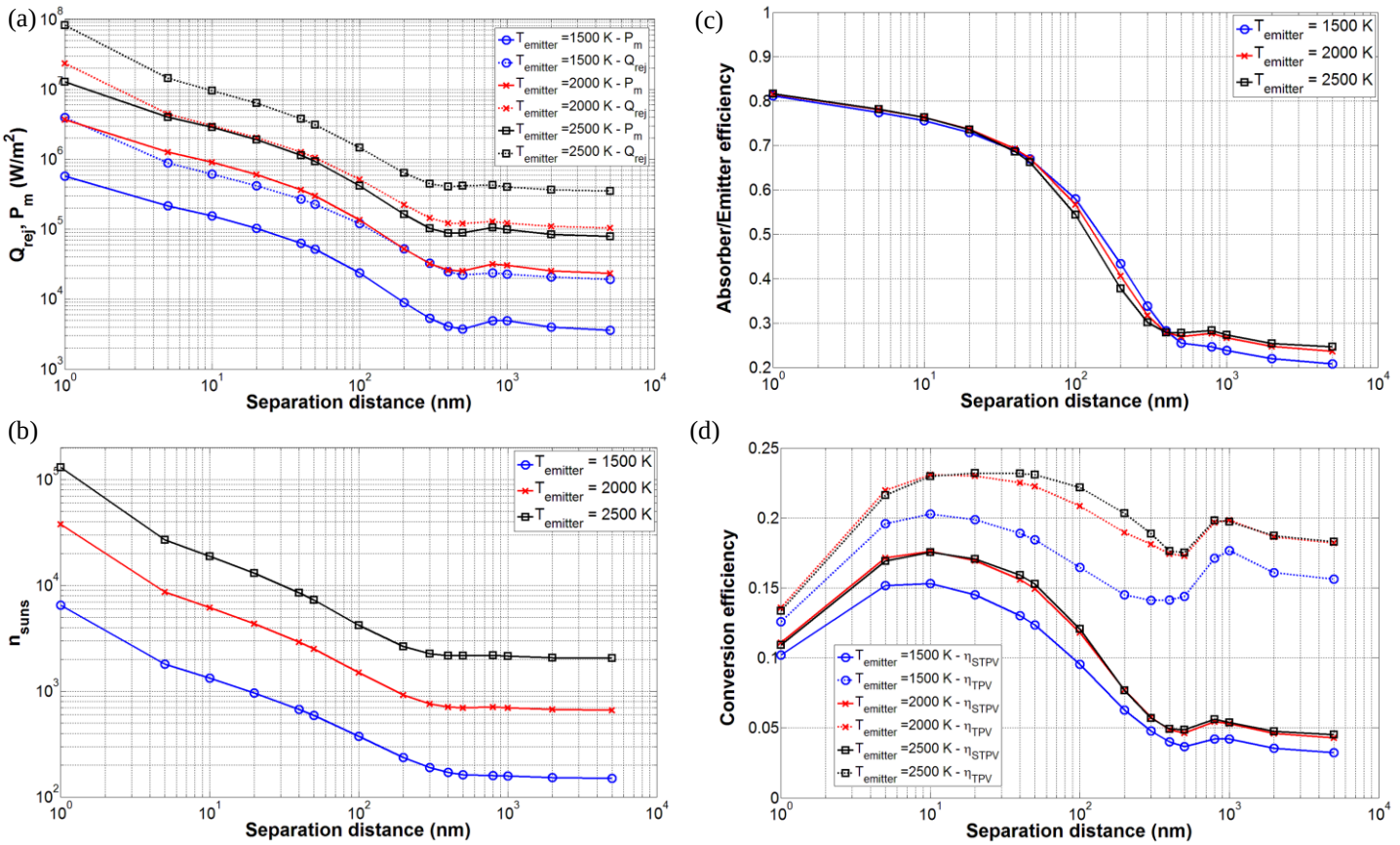

Fig. 3: Performance of near-field STPV as a function of separation distance and emitter temperature – a) Power output and heat rejected from near-field STPV, b) Number of suns (solar concentration) required by near-field STPV, c) Absorber emitter efficiency, d) Conversion efficiency of near-field TPV and near-field STPV

Total conversion efficiency of the near-field solar thermophotovoltaic cell is defined as the ratio between maximum output electrical power and solar incident power:

$$\eta_{STPV} = \frac{P_m}{Q_{solar,inc}} \tag{30}$$

Near-field calculations and thermal models were carried out using Matlab while COMSOL was employed to couple minority carrier diffusion equation with near-field calculations done by Matlab.

RESULTS AND DISCUSSION

Figure 3 shows the performance of near-field STPV as a function of separation distance and emitter temperature. As expected, the smaller the separation distance between the emitter and the PV cell, the higher the output power density due to the increased thermal radiation power tunneled from emitter to the PV cell (Fig. 3-a), the output power in near-field region may reach up to 100 times that of the far-field region. Unfortunately this increase in power density is accompanied by increased heat rejection (i.e., cooling requirement) due to various losses (i.e. non-radiative recombination and absorption of thermal radiation below band-gap energy). This cooling requirement may be prohibitive, however important progress have been recently achieved in the thermal management of high heat-flux microsystem [30], [31]. Rejected heat should contribute in increasing PV cell temperature, which can be estimated by methodology in [15] as this will affect system performance.

To achieve such high output power density for small separation distances, solar concentration should be high, and increases with the decrease in separation distance (Fig. 3-b). Fresnel lens technology can reach up to 4600× concentration ratio [1], so to achieve such high concentration ratios, more than one lens is needed.

Near-field effect on absorber/emitter thermal efficiency is prominent, without any special enclosure, this can be explained by considering constant absorber temperature with variable separation distance. Radiation losses to the environment depend on the absorber temperature so they will stay constant, but decreasing the separation distance increases thermal radiation transfer to the PV cell, and also increases the absorbed power from the sun, so efficiency increases with decreasing the separation distance (Fig. 3-c). Absorber/emitter thermal efficiency also depends on absorber temperature, it increases with absorber temperature in the far-field region and no defined trend in the near-field region. This is because both losses to the

environment and solar power absorbed increase with absorber temperature increase. It is worth noting that this temperature dependence decrease while decreasing separation distance due to increased thermal power tunneled to PV cell compared to power loss to the environment.

TPV and STPV conversion efficiency generally increase with decreasing separation distance because the thermal radiation spectrum matches better with quantum efficiency (Fig. 3-d) for low separation distance. The interesting region in near-field solar STPV is above the 10 nm (due to limitation of cooling capacity and concentration), so near-field STPV enhancement may be realized at the peak in conversion efficiency near the 10 nm separation distance where conversion efficiency increases from 4.3% for far-field to 17% for 10 nm separation distance.

CONCLUSIONS

This work investigates the performance of a near-field STPV system. The results revealed an increase of absorber thermal efficiency with decreasing separation distance, even without using any special enclosure. The conversion efficiency of near-field STPV exceeds the far field one significantly for low separation distance (< 800 nm), and its maximum value (17%) occurs around a separation distance of 10 nm. Such arrangement is not easy to establish due to enormous cooling load (4×10^6 W/m^2) at low PV cell temperature 300 K. Power density increases with the decrease of separating distance, it can reach up to 10^7 W/m^2, and it is 9×10^5 W/m^2 at optimum efficiency point. Near-field STPV offers advantage of increased power density and absorber emitter efficiency, while it imposes design complexity when it comes to thermal management and solar concentration.

ACKNOWLEDGMENTS

This work has been supported by a grant through the Nebraska Center for Energy Sciences Research (NCESR) with funds provided by Nebraska Public Power District (NPPD) to the University of Nebraska – Lincoln (UNL) No. 4200000844, and by funds from the Department of Mechanical and Materials Engineering and the College of Engineering at UNL, awarded to SN.

REFERENCES

[1] A. L. Luque and A. Viacheslav, *Concentrator Photovoltaics*, vol. 130. Berlin, Heidelberg: Springer Berlin Heidelberg, 2007.

[2] N.-P. Harder and P. W rfel, “Theoretical limits of thermophotovoltaic solar energy conversion,” *Semicond. Sci. Technol.*, vol. 18, no. 5, pp. S151–S157, May 2003.

[3] W. Shockley and H. J. Queisser, “Detailed Balance Limit of Efficiency of p-n Junction Solar Cells,” *J. Appl. Phys.*, vol. 32, no. 3, p. 510, Jun. 1961.

[4] A. Datas, “DEVELOPMENT OF SOLAR THERMOPHOTOVOLTAIC SYSTEMS,” Technical University of Madrid, 2011.

[5] H. Yugami, H. Sai, K. Nakamura, N. Nakagawa, and H. Ohtsubo, “Solar thermophotovoltaic using Al_2O_3 / Er_3/Al_5/O_12 eutectic composite selective emitter,” in *Conference Record of the Twenty-Eighth IEEE Photovoltaic Specialists Conference - 2000 (Cat. No.00CH37036)*, 2000, pp. 1214–1217.

[6] A. Lenert, D. M. Bierman, Y. Nam, W. R. Chan, I. Celanović, M. Soljačić, and E. N. Wang, “A nanophotonic solar thermophotovoltaic device.,” *Nat. Nanotechnol.*, vol. 9, no. 2, pp. 126–30, Feb. 2014.

[7] A. Lenert, V. Rinnerbauer, D. M. Bierman, Y. Nam, I. Celanovic, M. Soljacic, and E. N. Wang, “2D Photonic-crystals for high spectral conversion efficiency in solar thermophotovoltaics,” in *2014 IEEE 27th International Conference on Micro Electro Mechanical Systems (MEMS)*, 2014, pp. 576–579.

[8] V. Rinnerbauer, S. Ndao, Y. X. Yeng, W. R. Chan, J. J. Senkevich, J. D. Joannopoulos, M. Soljačić, and I. Celanovic, “Recent developments in high-temperature photonic crystals for energy conversion,” *Energy Environ. Sci.*, vol. 5, no. 10, p. 8815, Sep. 2012.

[9] A. Kittel, W. Müller-Hirsch, J. Parisi, S.-A. Biehs, D. Reddig, and M. Holthaus, “Near-Field Heat Transfer in a Scanning Thermal Microscope,” *Phys. Rev. Lett.*, vol. 95, no. 22, p. 224301, Nov. 2005.

[10] L. Hu, A. Narayanaswamy, X. Chen, and G. Chen, “Near-field thermal radiation between two closely spaced glass plates exceeding Planck’s blackbody radiation law,” *Appl. Phys. Lett.*, vol. 92, no. 13, p. 133106, Apr. 2008.

[11] S. Shen, A. Narayanaswamy, and G. Chen, “Surface phonon polaritons mediated energy transfer between nanoscale gaps.,” *Nano Lett.*, vol. 9, no. 8, pp. 2909–13, Aug. 2009.

[12] R. S. DiMatteo, “Micron-gap ThermoPhotoVoltaics (MTPV),” in *AIP Conference Proceedings*, 2003, vol. 653, pp. 232–240.

[13] S. Basu, Z. M. Zhang, and C. J. Fu, “Review of near-field thermal radiation and its application to energy conversion,” *Int. J. Energy Res.*, vol. 33, no. 13, pp. 1203–1232, Oct. 2009.

[14] T. J. Bright, L. P. Wang, and Z. M. Zhang, "Performance of Near-Field Thermophotovoltaic Cells Enhanced With a Backside Reflector," *J. Heat Transfer*, vol. 136, no. 6, p. 062701, Mar. 2014.

[15] M. Francoeur, R. Vaillon, and M. P. Mengüç, "Thermal Impacts on the Performance of Nanoscale-Gap Thermophotovoltaic Power Generators," *IEEE Trans. Energy Convers.*, vol. 26, no. 2, pp. 686–698, Jun. 2011.

[16] J. R. Howell, R. Siegel, and M. P. Menguc, *Thermal Radiation Heat Transfer, 5th Edition [Hardcover]*. CRC Press; 5 edition, 2010, p. 987.

[17] Z. Zhang, *Nano/Microscale Heat Transfer*. McGraw-Hill Professional; 1 edition, 2007, p. 479.

[18] S. M. Rytov, Y. A. Kravtsov, and V. I. Tatarskii, *Principles of Statistical Radiophysics*. Springer-Verlag, 1989.

[19] A. Narayanaswamy and G. Chen, "DIRECT COMPUTATION OF THERMAL EMISSION FROM NANOSTRUCTURES - Begell House Digital Library," *Annu. Rev. Heat Transf.*, vol. XIV, no. 14, pp. 169–195, 2005.

[20] M. Francoeur and M. Pinar Mengüç, "Role of fluctuational electrodynamics in near-field radiative heat transfer," *J. Quant. Spectrosc. Radiat. Transf.*, vol. 109, no. 2, pp. 280–293, Jan. 2008.

[21] G. Chen and G. C. PhD., *Nanoscale Energy Transport and Conversion: A Parallel Treatment of Electrons, Molecules, Phonons, and Photons*. Oxford University Press, 2005, p. 531.

[22] M. Francoeur, "NEAR-FIELD RADIATIVE TRANSFER: THERMAL RADIATION, THERMOPHOTOVOLTAIC POWER GENERATION AND OPTICAL CHARACTERIZATION," University of Kentucky Doctoral Dissertation, 2010.

[23] E. D. Palik, *Palik, Handbook of Optical Constants of Solids, Vol.2*, vol. 2. 1991.

[24] J. A. Gonzalez-Cuevas, T. F. Refaat, M. N. Abedin, and H. E. Elsayed-Ali, "Calculations of the temperature and alloy composition effects on the optical properties of Al_ x Ga_(1−x) As_y Sb_(1−y) and Ga_x In_(1−x) As_y Sb_(1−y) in the spectral range 0.5–6 eV," *J. Appl. Phys.*, vol. 102, no. 1, p. 014504, Jul. 2007.

[25] S. Adachi, *Optical Constants of Crystalline and Amorphous Semiconductors: Numerical Data and Graphical Information*. Norwell: Kluwer Academic Publishers, 1999.

[26] K. Park, S. Basu, W. P. King, and Z. M. Zhang, "Performance analysis of near-field thermophotovoltaic devices considering absorption distribution," *J. Quant. Spectrosc. Radiat. Transf.*, vol. 109, no. 2, pp. 305–316, Jan. 2008.

[27] T. F. Refaat, "Modeling of the temperature-dependent spectral response of In_(1-x) Ga_x Sb infrared photodetector," *Opt. Eng.*, vol. 45, no. 4, p. 044001, Apr. 2006.

[28] B. G. Streetman and S. K. Banerjee, *Solid State Electronic Devices*, vol. 10. 2006, p. 581.

[29] R. Vaillon, L. Robin, C. Muresan, and C. Ménézo, "Modeling of coupled spectral radiation, thermal and carrier transport in a silicon photovoltaic cell," *Int. J. Heat Mass Transf.*, vol. 49, no. 23–24, pp. 4454–4468, Nov. 2006.

[30] S. Ndao, Y. Peles, and M. K. Jensen, "Experimental investigation of flow boiling heat transfer of jet impingement on smooth and micro structured surfaces," *Int. J. Heat Mass Transf.*, vol. 55, no. 19–20, pp. 5093–5101, Sep. 2012.

[31] S. Ndao, H. J. Lee, Y. Peles, and M. K. Jensen, "Heat transfer enhancement from micro pin fins subjected to an impinging jet," *Int. J. Heat Mass Transf.*, vol. 55, no. 1–3, pp. 413–421, Jan. 2012.